Finite-temperature phase diagram of the t-J model: Renormalization-group theory

Alexis Falicov and A. Nihat Berker
Department of Physics, Massachusetts Institute of Technology, Cambridge, Massachusetts 02139
(Received 10 December 1993)

The finite-temperature phase diagram of the t-J model of electronic conduction is calculated in d dimensions, using the Migdal-Kadanoff renormalization-group procedure. No finite-temperature phase transition in $d=1$ and a finite-temperature first-order boundary ending at a critical point in $d=2$ are found. In $d=3$, a remarkably complex multicritical phase diagram is found, with a new phase, between hole dopings of 0.3 and 0.4 and temperatures $1/J$ below 0.4, in which the hopping strength t renormalizes to infinity under rescaling. Our results are confirmed by comparison of calculated electron densities, kinetic energies, and nearest-neighbor density-density and spin-spin correlation functions with exact finite-cluster results.

The metal-insulator transition,[1] metallic magnetism,[2] heavy-fermion behavior,[3,4] and high-T_c superconductivity[5] are all finite-temperature effects that result from the strong correlation of electrons in narrow energy bands. It is therefore of significant interest to study finite-temperature phenomena in strongly correlated electronic systems. Accordingly, we have performed the finite-temperature statistical mechanics of the t-J model of electronic conduction in d dimensions, obtaining the phase diagrams, electron densities, kinetic energies, and nearest-neighbor correlation functions, using the Migdal-Kadanoff renormalization-group procedure. No finite-temperature phase transition in $d=1$ and a finite-temperature critical point terminating a first-order boundary in $d=2$ are found. In $d=3$, a remarkably complex multicritical phase diagram, with a new phase and multiple reentrances at different temperature scales, is found. Electron densities, kinetic energies, and nearest-neighbor density-density and spin-spin correlation functions calculated by renormalization-group theory are supported by finite-cluster results.

Our renormalization-group calculation automatically yields the global finite-temperature phase diagram and statistical mechanics of a generalized t-J model, defined, on a lattice with one spherically symmetric orbital at each site i, by the following Hamiltonian:

$$-\beta\mathcal{H}=P\left[-t\sum_{\langle ij\rangle,\sigma}(c_{i\sigma}^{\dagger}c_{j\sigma}+c_{j\sigma}^{\dagger}c_{i\sigma})-J\sum_{\langle ij\rangle}\mathbf{S}_i\cdot\mathbf{S}_j+V\sum_{\langle ij\rangle}n_in_j+\mu\sum_i n_i\right]P\ , \tag{1}$$

where $c_{i\sigma}^{\dagger}$ and $c_{i\sigma}$ are the creation and annihilation operators for an electron in the Wannier state at i with z component of spin $\sigma=\downarrow$ or $\uparrow$, $n_{i\sigma}=c_{i\sigma}^{\dagger}c_{i\sigma}$ and $\mathbf{S}_i$ are electron density and spin operators at site i, and $n_i=n_{i\uparrow}+n_{i\downarrow}$. The projection operator $P=\prod_i(1-n_{i\downarrow}n_{i\uparrow})$ projects out all states with any doubly occupied site. The traditional t-J Hamiltonian is a special case of Eq. (1), obtained for $V/J=0.25$. The Hamiltonian of Eq. (1) describes the hopping of electrons (first term), which interact through both a nearest-neighbor antiferromagnetic coupling (for $J>0$) and a nearest-neighbor Coulomb interaction (V term). On bipartite lattices (i.e., lattices that can be separated into two sublattices such that any two nearest-neighbors are on different sublattices), the sign of t in the partition function can be reversed by a simple redefinition of the phase of the Wannier states on one sublattice. Thus, with no loss of generality, we restrict to $t>0$.

While zero-temperature properties of the t-J model have been studied by mean-field theory,[5,6] small-cluster calculations,[7] and Bethe ansatz,[8] the finite-temperature behavior of the model is largely unexplored,[9] especially in $d=3$ where we now obtain a rich structure. The position-space renormalization-group method is well suited for the latter task. Our approach starts with an approximate decimation in $d=1$, which is then developed onto higher dimensions by the Migdal-Kadanoff procedure. Determination of the global connectivity of the flows also determines the global phase diagram, a cross section of which applies to the traditional t-J model. Summation along entire renormalization-group trajectories yields the finite-temperature free energy, electron density, kinetic energy, and nearest-neighbor correlation functions.

In $d=1$, the Hamiltonian can be rewritten as

$$-\beta\mathcal{H}=\sum_i[-\beta\mathcal{H}(i,i+1)]\ . \tag{2}$$

Because of the noncommutativity of quantum operators, it is impossible to carry out exactly the decimation, even in one dimension. We therefore use an approximation, previously used[10,11] on quantum spin systems:

0163-1829/95/51(18)/12458(6)/$06.00

$$\mathrm{Tr}_{\mathrm{odd}}\exp\{-\beta\mathcal{H}\}=\mathrm{Tr}_{\mathrm{odd}}\exp\left\{\sum_i[-\beta\mathcal{H}(i,i+1)]\right\}\approx\mathrm{Tr}_{\mathrm{odd}}\prod_i\exp\{-\beta\mathcal{H}(2i,2i+1)-\beta\mathcal{H}(2i+1,2i+2)\}$$

$$=\prod_i\exp\{-\beta'\mathcal{H}'(2i,2i+2)\}\approx\exp\left\{\sum_i[-\beta'\mathcal{H}'(2i,2i+2)]\right\}=\exp\{-\beta'\mathcal{H}'\}\ , \tag{3}$$

where the primes refer to the renormalized system, all summations and products are over all integer values of i, and $\mathrm{Tr}_{\mathrm{odd}}$ indicates a trace over the degrees of freedom at all odd-numbered sites. The approximation of Eq. (3) consists in ignoring, in two formally opposite directions (therefore, hopefully, with some mutual compensation), the noncommutations of operators beyond two consecutive segments of the unrenormalized system. Quantum effects are thus taken into account, at each rescaling, within clusters formed by two consecutive segments. This procedure becomes exact in the high-temperature limit $\beta\to 0$ (since the commutators are proportional to β^2) and is thought to shed light on the finite-temperature behavior, as has been validated in quantum spin systems[10,11] and a very ample contingent of classical systems using similarly uncontrolled, but successful, local approximations in position-space renormalization group.[12–14]

Our Migdal-Kadanoff renormalization-group procedure for higher dimensions is composed of a "bond-moving" step, which has the effect of leaving, on linear segments, interactions strengthened by a factor of $f\geq 1$, followed by a decimation (here as described above), followed by a strengthening of the interactions by a factor of $f^{-1}b^{d-1}\geq 1$. The length rescaling factor is $b=2$. These choices of interaction strengthening factors guarantee that every interaction term that is omitted is accounted by interaction strengthening. This is necessary for the required eigenvalue $\lambda=b^d$ of the renormalization-group transformation linearized at any fixed point. The corresponding left eigenvector is composed of the densities at the fixed point, which in turn determine all densities in the entire thermodynamic space. While all previous Migdal-Kadanoff[15,16] renormalization-group studies have used the extremes of $f=1$ or b^{d-1}, we note here that any choice in the range $1\leq f\leq b^{d-1}$ is equally plausible. The calculated critical exponents, phase diagram topologies, and thermodynamic densities are not affected by the choice of f, whereas the interaction strengths at the phase boundaries are inversely proportional to f. In this study, the value of f is fixed so that the correct critical temperature of the Ising model is obtained, which dictates $f=1.4024$ in $d=2$ and $f=1.2279$ in $d=3$.

The renormalization-group transformation maps an initial system onto one with identical structure, thinned out degrees of freedom, and "renormalized" values[17] of the interaction constants appearing in the Hamiltonian of Eq. (1). The latter values are determined by "recursion relations" based on the implementation of Eq. (3). These recursion relations are obtained here, after some complicated algebra, in closed form. The bond-moved interaction strengths are

$$\tilde{t}=ft,\quad \tilde{J}=fJ,\quad \tilde{V}=fV,\quad \tilde{\mu}=f\mu\ . \tag{4}$$

Letting

$$\begin{aligned}&v=\exp(-\tilde{J}/8+\tilde{V}/2+\tilde{\mu}/4d),\\&x=\exp(3\tilde{J}/8+\tilde{V}/2+\tilde{\mu}/4d),\quad u=\exp(\tilde{\mu}/4d)\ ,\\&f(A)\equiv(A/\sqrt{2\tilde{t}^2+A^2})\sinh\sqrt{2\tilde{t}^2+A^2}\\&\qquad+\cosh\sqrt{2\tilde{t}^2+A^2}\ ,\end{aligned} \tag{5}$$

and

$$\begin{aligned}&\gamma_1=1+2u^3f(\tilde{\mu}/4d)\ ,\\&\gamma_2=(1/2)x^2u^2+uf(-\tilde{\mu}/4d)\\&\qquad+(3/2)vu^2f(-\tilde{J}/8+\tilde{V}/2+\tilde{\mu}/4d)\ ,\\&\gamma_3=(4/3)v^4+(2/3)vx^3+vf(\tilde{J}/8-\tilde{V}/2-\tilde{\mu}/4d)\ ,\\&\gamma_4=1+(3/2)v^2u^2+(1/2)xu^2f(3\tilde{J}/8+\tilde{V}/2+\tilde{\mu}/4d)\ ,\\&\gamma_5=2v^3x+xf(-3\tilde{J}/8-\tilde{V}/2-\tilde{\mu}/4d)\ ,\end{aligned} \tag{6}$$

the renormalized interaction constants are

$$\begin{aligned}&t'=f^{-1}b^{d-1}(1/2)\ln(\gamma_4/\gamma_2)\ ,\\&J'=f^{-1}b^{d-1}\ln(\gamma_5/\gamma_3)\ ,\\&V'=f^{-1}b^{d-1}[\ln(\gamma_1\gamma_3/\gamma_2\gamma_4)+(1/4)\ln(\gamma_5/\gamma_3)]\ ,\\&\mu'=f^{-1}b^{d-1}[\tilde{\mu}+2d\ln(\gamma_2\gamma_4/\gamma_1^2)]\ ,\\&G'=f^{-1}b^{d-1}[bfG+\ln(\gamma_1)]\ ,\end{aligned} \tag{7}$$

where G is the additive constant per bond in the Hamiltonian. It incorporates the free-energy contributions from the smaller length scales that have been eliminated under rescaling. Note that the subspaces $t=0$, $J=0$, and $t=J=V=0$ are each closed under the renormalization-group transformation, as expected by the fact that missing more complicated couplings should not be generated by rescaling. Closed-form recursion relations are necessary to calculate electron densities, kinetic energies, and nearest-neighbor correlation functions.

Our renormalization-group calculation indicates that no finite-temperature phase transition occurs in $d=1$ and that a finite-temperature first-order boundary[18] terminating at a critical point[19,9] occurs in $d=2$, as shown in Fig. 1.

Before proceeding to $d=3$, we note that in the past new global phase diagrams obtained by approximate renormalization-group calculations have been given credence by the correct rendition of the special cases of the system solved.[13] In the present case, Eq. (1) reduces to the quantum Heisenberg magnet for $\mu\to\infty$, to the Ising magnet in a field for $t=J=0$, and to the vectorialized Blume-Emery-Griffiths (BEG) model[20] in its quantum version for $t=0$. Indeed, in the $d=1,2$ Heisenberg

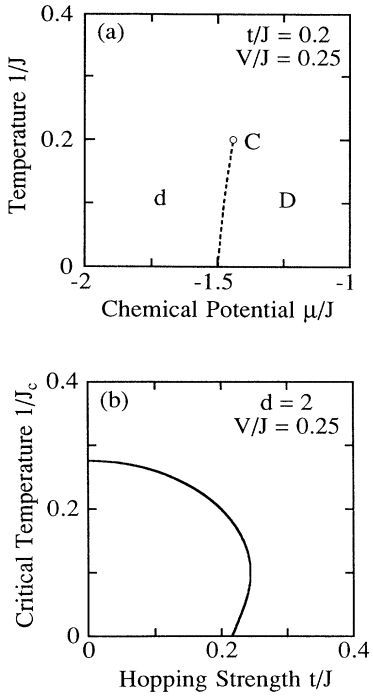

FIG. 1. (a) Typical cross section of the calculated global finite-temperature phase diagram of the two-dimensional t-J model, with $t/J=0.2$ and $V/J=0.25$. Dense disordered (D) and dilute disordered (d) phases are separated by a first-order phase boundary terminating at a critical point (C). (b) Calculated critical temperatures $1/J_c$ as a function of relative hopping strength t/J, in two dimensions. It is thus seen that finite-temperature phase separation occurs only for low values of t/J.

subspaces of the model, our calculation yields no finite-temperature phase transition. In the $d=3$ Heisenberg subspace, it yields low-temperature antiferromagnetically (for $J>0$) or ferromagnetically ($J<0$) ordered phases, each separated by a second-order transition from the high-temperature disordered phase. The antiferromagnetic transition temperature is calculated here to be 1.22 times the ferromagnetic transition temperature, to be compared with the value of 1.14 for this ratio from series expansion.[21] All of the latter behavior, as well as the behavior of the Ising model with field and the multicritical global phase diagram of the quantum BEG model support the validity of the global calculation.

Returning to the generalized t-J model of Eq. (1), a novel and intricate global phase diagram is obtained in $d=3$. This is conveyed in Figs. 2 and 3. To explain it, we start with $t=0$ [Figs. 2(a)–(c)], where the model reduces to the quantum vectorialized BEG model. In this subspace, constant V/J phase diagram cross sections in the variables of $1/J$ (proportional to temperature) and μ/J (proportional to dimensionless chemical potential) exhibit antiferromagnetic (a), dense disordered (D), and dilute disordered (d) phases separated by first- and second-order phase boundary lines. These lines are punctuated by critical points (C) and critical end-points (E) for $V/J>0.25$ [e.g., Fig. 2(a)], tricritical points (T) for $V/J<0.25$ [e.g., Fig. 2(c)], and a special multicritical point (M) for $V/J=0.25$ [Fig. 2(b)]. The latter point is a quantum analog for the classical three-state Potts point.[13] With the further refinement of renormalization-group theory by the inclusion of effective vacancies[14] to represent, in the renormalized systems, the short-range disorder of the finer length scales, this multicritical point M could be replaced by a structure including a tricritical point, a triple point, and a critical point, with a range of occurrence[13] about $V/J=0.25$.

The new phase-diagram phenomena appear for $t\neq 0$, as might be expected, since the model becomes a true conduction–coupled order-parameter model. The critical temperature of the antiferromagnetic transition of the filled system is 43% lower than the series expansion value.[22] The antiferromagnetic phase of the filled system is unstable to a small amount of doping by holes (by about 5% in Fig. 3). One novel aspect is the appearance, close to the phase separation boundary [dashed curves in Figs. 2(d) and 3], of a new phase (which we shall call "τ"), seen, for example, in Figs. 2(d) and 3 for $t/J=2.25$ and $V/J=0.25$, which applies to the traditional t-J model. This phase, to our knowledge never seen before in finite-temperature phase transition theories, is the only volume of the extended phase diagram in which, after multiple rescalings, the hopping strength t does *not* renormalize to zero. In fact, all the interaction constants (t,J,V,μ) renormalize to infinite strengths, while their ratios eventually remain constant at $J/t=2$, $V/t=3/2$, $\mu/t=-6$, and $t\to\infty$, a typical behavior for the renormalization-group sink[13] of a low-temperature phase. A distinctive feature is that at this sink, which as usual epitomizes the entire thermodynamic phase that it attracts, the electron density $\langle n_i\rangle$, obtained as usual from the left eigenvector with eigenvalue b^d of the recursion matrix, has the non-unit, nonzero value of $\langle n_i\rangle^*=2/3$. This feature makes strong-coupling conduction possible by having the system nonfull and nonempty of electrons, and has also not been seen previously, to our knowledge.

Another feature is the appearance of several islands of the antiferromagnetic phase, as seen in Figs. 2(d) and 3. The islands are bounded by first- and second-order phase transitions adorned by the various special points already mentioned above. Thus, a multiply reentrant phase diagram topology obtains. The antiferromagnetic phase also occurs as a narrow sliver, within the disordered phase reaching zero temperature between the antiferromagnetic and τ phases. The appearance of the antiferromagnetic islands at dopings in the neighborhood of the τ phase (see Fig. 3) indicates that, when the hopping strength t increases under rescaling, antiferromagnetically long-range correlated states acquire substantial off-diagonal elements, which lowers the free energy of the antiferromagnetic phase.

The transition between the new τ and disordered phases is second-order, controlled by a redundant triplet structure of fixed points at $(t^*,J^*,V^*,\mu^*)=(0.84, 1.22, -2.23, 12.91)$, $(0.69, 1.38, -1.03, 4.15)$, $(0.74, 3.42, -2.08, 1.52)$ with the respective relevant eigenvalue exponents $y=1.001$, 0.993, 1.009, corresponding to the critical exponents $\nu=0.999$ and $\alpha=-0.997$. Although

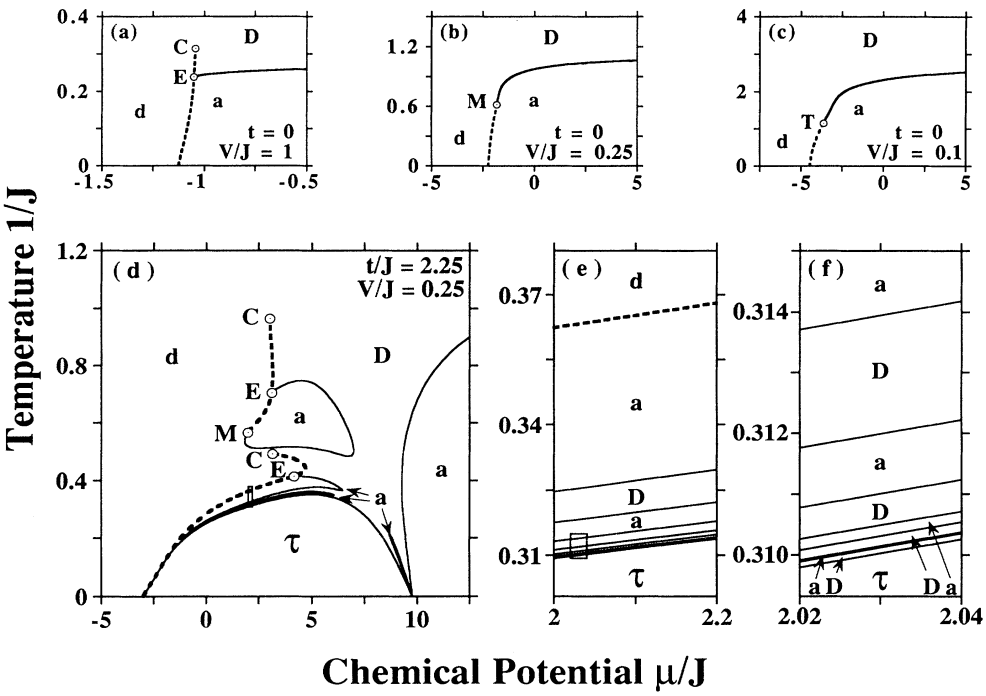

FIG. 2. Typical cross sections of the calculated global finite-temperature phase diagram for the three-dimensional t-J model, in temperature and chemical potential variables. Antiferromagnetic (a), dense disordered (D), and dilute disordered (d) phases and the new "τ" phase are separated by first-order (dashed curves) and second-order (full curves) boundaries punctuated by critical points (C), critical end-points (E), tricritical points (T), and multicritical points (M). (e) and (f) are, respectively, the blowups of the small rectangles in (d) and (e). The temperature versus electron-density phase diagram corresponding to (d) is in Fig. 3.

the latter numbers are to be taken only as indicative, in view of the approximations, the fact that the eigenvalue exponents of the three redundant fixed points are so close to each other points to internal consistency in the calculation. On the less dense side of the boundary of the τ phase, a "lamellar" sequence of antiferromagnetic slivers and disordered inlets occurs, at several temperature scales, as seen in Figs. 2(e) and 2(f).

Our results on the finite-temperature phase diagram of the t-J model can be categorized as follows:

(1) At the coarsest temperature scale, a new τ phase occurs as a distinct thermodynamic phase in a narrow interval, e.g., between 30 and 40 % doping and at temperatures $1/J < 0.4$ in Fig. 3. The antiferromagnetic phase of the filled system is unstable to a small amount of doping (about 5% in Fig. 3), but the antiferromagnetic long-range correlations are enhanced in the neighborhood of the τ phase.

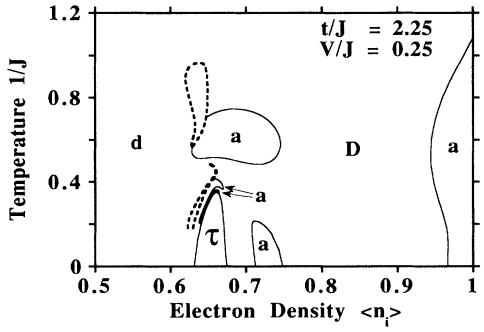

FIG. 3. Typical cross section of the calculated global finite-temperature phase diagram for the three-dimensional t-J model, in temperature and electron-density variables. The coexistence boundaries of the first-order phase transitions are drawn with dashed curves; the unmarked regions inside these boundaries are the coexistence regions of the phases marked at each side of the regions. The second-order phase boundaries are drawn with full curves. The temperature versus chemical potential phase diagram corresponding to this figure is in Fig. 2(d).

(2) Islands of the antiferromagnetic phase appear within the disordered phase.

(3) On the less dense side of the boundary of the τ phase, a fine structure of narrow antiferromagnetic slivers and narrow disordered inlets occur at several temperature scales.

It would be most interesting to know whether these new results survive the removal or lessening of the approximations made here. Our treatment is, of course, an approximate study of the t-J model, due to the mistreatment of some of the commutation relations [Eq. (3)] and due to the Migdal-Kadanoff bond moving. Our treatment is also, simultaneously, a lesser approximation to the statistical mechanics of the t-J model on a d-dimensional hierarchical lattice:[23] Bond moving is exact, but the mistreatment of some of the commutation relations remains. It would be rewarding if the new phase diagram survives at least for the physical realization of the t-J model on hierarchical lattices.

We have calculated electron densities, average kinetic energies per nearest-neighbor site pairs,

$$\langle T_{ij} \rangle = \langle c_{i\uparrow}^{\dagger} c_{j\uparrow} + c_{j\uparrow}^{\dagger} c_{i\uparrow} + c_{i\downarrow}^{\dagger} c_{j\downarrow} + c_{j\downarrow}^{\dagger} c_{i\downarrow} \rangle \ , \tag{8}$$

and nearest-neighbor density-density and spin-spin correlation functions by summing along renormalization-group trajectories and matching to the densities of phase sinks.[23] We have also calculated the same quantities for a small cluster of four sites with bipartite periodic boundary conditions (Fig. 4 inset). The latter quantities should not contain the nonanalyticities of phase transitions, but

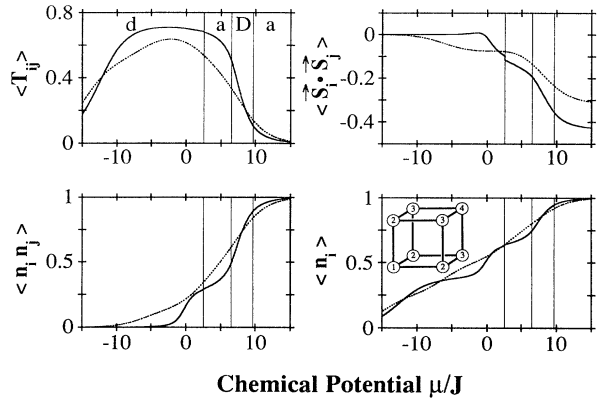

FIG. 4. Electron densities, kinetic energies, and nearest-neighbor density-density and spin-spin correlation functions at constant temperature $1/J=0.61$ as a function of chemical potential, across the phase diagram of Fig. 2(d) which has $t/J=2.25$ and $V/J=0.25$. The vertical lines in this figure indicate the location of the phase transitions. The phases are labeled in the first panel. Quantitative trends in the calculated renormalization-group (full curves) and finite-cluster (dotted curves) show agreement. Part of the bipartite finite cluster of four sites with periodic boundary conditions is shown in the last panel. The ferromagnetic nearest-neighbor correlation, $\mathbf{S}_i \cdot \mathbf{S}_j > 0$, in the disordered phase is even more apparent in Fig. 7.

are expected to be of comparable value to the infinite-system quantities. Thus, to gauge the accuracy of our approximation, trends in the renormalization-group results for the electron densities, kinetic energies, and nearest-neighbor correlation functions are compared to the finite-cluster results in Figs. 4, 5, and 6. Good agreement is seen for these quantitative trends, even at low temperatures. The kinetic energies and nearest-neighbor correlation functions are given as functions of densities in Figs. 6

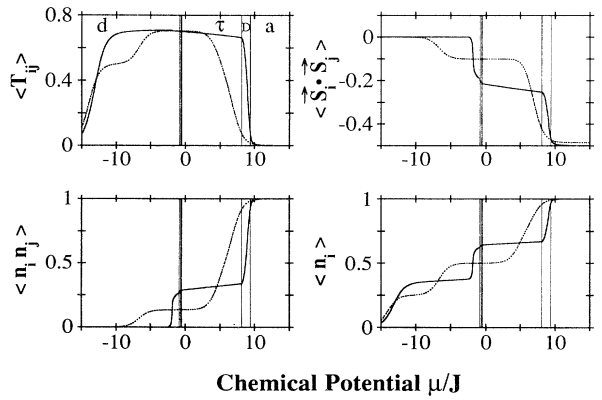

FIG. 5. Same as Fig. 4, but with the lower temperature $1/J=0.23$. In this figure, when it is realized that the finite-cluster and renormalization-group curves are shifted, good agreement is seen in the trends, even at the low temperature of this figure.

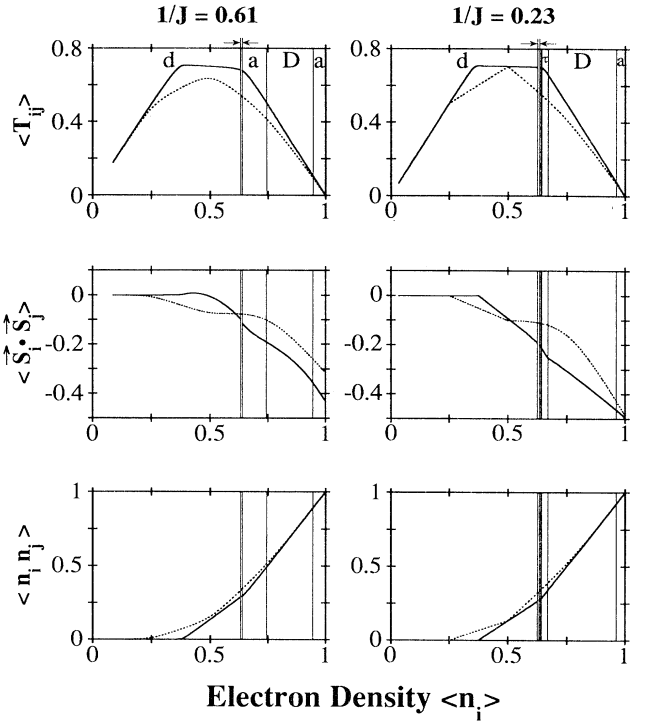

FIG. 6. Kinetic energies and nearest-neighbor density-density and spin-spin correlation functions at constant temperatures $1/J=0.61$ and 0.23 as a function of electron density, corresponding to Figs. 4 and 5. The kinetic energy, proportional to conductivity [Eq. (9)], as expected goes to zero in the dilute and dense limits. Arrows indicate the (small) range of forbidden densities due to the discontinuity at the first-order transition from the dilute disordered phase.

and 7. The kinetic energies reflect the conductivity of the system as seen from the sum rule[24]

$$\mathrm{tr}\int_0^\infty dw\ \mathrm{Re}[\sigma_{uu}(w)] = -\frac{\pi e^2 d}{2\hbar a}\langle T_{ij}\rangle\ , \tag{9}$$

where $\sigma_{uu}(w)$ is the frequency-dependent conductivity, e is the electronic charge, and a is the lattice spacing. Thus, the conductivity, as expected, goes to zero in the

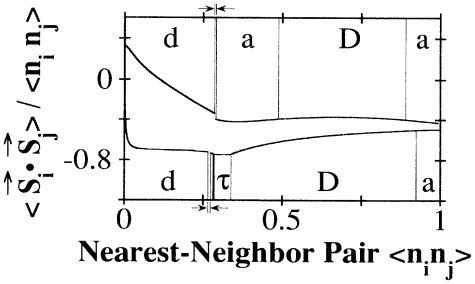

FIG. 7. Nearest-neighbor spin-spin correlations per nearest-neighbor electrons. The upper and lower curves, respectively, correspond to $1/J=0.61$ and 0.23. Note the ferromagnetic correlations at low pair densities.

dilute and dense limits. Figure 7 exhibits nearest-neighbor ferromagnetic correlations in the low pair-density regime. Similar short-range ferromagnetic correlations have been obtained previously in exact finite-cluster diagonalizations.[25,26]

We thank Efthimios Kaxiras, Patrick Lee, Karin Rabe, Maurice Rice, and Manfred Sigrist for useful conversations. This research was supported by the JSEP Contract No. DAAL 03-92-C0001. A.F. acknowledges partial support from the NSF.

[1]N. F. Mott, Rev. Mod. Phys. **40**, 677 (1968).
[2]F. C. Zhang and T. M. Rice, Phys. Rev. B **37**, 3759 (1988).
[3]G. R. Stewart, Rev. Mod. Phys. **56**, 765 (1984).
[4]P. Fulde, J. Keller, and G. Zwicknagl, *Solid State Physics: Advances in Research and Applications,* edited by H. Ehrenreich and D. Turnbull (Academic, New York, 1988), Vol. 41, p. 1.
[5]P. W. Anderson, Science **235**, 1196 (1987).
[6]G. Baskaran, Z. Zhou, and P. W. Anderson, Solid State Commun. **63**, 973 (1987).
[7]J. K. Freericks and L. M. Falicov, Phys. Rev. B **42**, 4960 (1990).
[8]P.A. Bares, G. Blatter, and M. Ogata, Phys. Rev. B **44**, 130 (1991).
[9]One previous calculation is S. A. Cannas and C. Tsallis, Phys. Rev. B **46**, 6261 (1992). These authors did not derive the closed-form recursion relations, but implemented them numerically. They did not obtain the new phase, the corresponding phase diagram structure, the electron densities, kinetic energies, and correlation functions obtained here.
[10]M. Suzuki and H. Takano, Phys. Lett. A **69**, 426 (1979).
[11]H. Takano and M. Suzuki, J. Stat. Phys. **26**, 635 (1981).
[12]Th. Niemeijer and J. M. J. van Leeuwen, Phys. Rev. Lett. **31**, 1411 (1973).
[13]A. N. Berker and M. Wortis, Phys. Rev. B **14**, 4946 (1976).
[14]B. Nienhuis, A. N. Berker, E. K. Riedel, and M. Schick, Phys. Rev. Lett. **43**, 737 (1979).
[15]A. A. Migdal, Zh. Eksp. Teor. Fiz. **69**, 1457 (1975) [Sov. Phys. JETP **42**, 743 (1976)].
[16]L. P. Kadanoff, Ann. Phys. (N.Y.) **100**, 359 (1976).
[17]Note that after the first renormalization, the system is quantitatively mapped onto one consisting of sites from only one of the two sublattices of the original system. Ferromagnetic couplings between these sites are perfectly consistent with antiferromagnetic order in the original system, as can be seen from the calculated nearest-neighbor correlation function $\mathbf{S}_i \cdot \mathbf{S}_j$ in Figs. 4, 5, and 6. The latter calculation establishes the antiferromagnetism of the original system with no ambiguity. Under the first renormalization, the critical point of the totally filled antiferromagnetic system maps onto the critical point of the totally filled ferromagnetic system. The antiferromagnetic critical temperature is thus here calculated to be 1.22 times the ferromagnetic critical temperature, to be compared with the value of 1.14 for this ratio from series expansion (Ref. 21).
[18]S. A. Kivelson, V. J. Emery, and H. Q. Lin, Phys. Rev. B **42**, 6523 (1990).
[19]W. O. Putikka, M. U. Luchini, and T. M. Rice, Phys. Rev. Lett. **68**, 538 (1992).
[20]A. N. Berker and D. R. Nelson, Phys. Rev. B **19**, 2488 (1979).
[21]G. S. Rushbrooke and P. J. Wood, Mol. Phys. **6**, 409 (1963).
[22]G. S. Rushbrooke, G. A. Baker, Jr., and P. J. Wood, in *Phase Transitions and Critical Phenomena,* edited by C. Domb and M. S. Green (Academic, New York, 1984), Vol. 3, p. 306.
[23]A. N. Berker and S. Ostlund, J. Phys. C **12**, 4961 (1979).
[24]D. Baeriswyl, C. Gros, and T. M. Rice, Phys. Rev. B **35**, 8391 (1987).
[25]E. Kaxiras and E. Manousakis, Phys. Rev. B **37**, 656 (1988).
[26]E. Kaxiras and E. Manousakis, Phys. Rev. B **38**, 866 (1988).